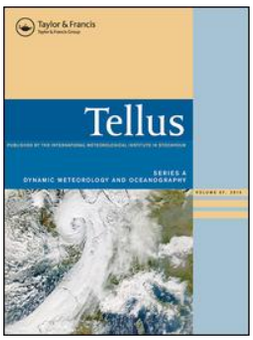

Tellus A: Dynamic Meteorology and Oceanography

ISSN: (Print) 1600-0870 (Online) Journal homepage: http://www.tandfonline.com/loi/zela20

The feedback of midlatitude waves onto the Hadley cell in a simple general circulation model

E. Becker, G. Schmitz & R. Geprägs

To cite this article: E. Becker, G. Schmitz & R. Geprägs (1997) The feedback of midlatitude waves onto the Hadley cell in a simple general circulation model, Tellus A: Dynamic Meteorology and Oceanography, 49:2, 182-199, DOI: 10.3402/tellusa.v49i2.14464

To link to this article: https://doi.org/10.3402/tellusa.v49i2.14464

Tellus (1997), 49A, 182–199
Printed in UK — all rights reserved

TELLUS
ISSN 0280–6495

The feedback of midlatitude waves onto the Hadley cell in a simple general circulation model

By E. BECKER,* G. SCHMITZ AND R. GEPRÄGS, [1]*Institute of Atmospheric Physics, Schloßstraße 4–6, D-18225 Kühlungsborn, Germany*

(Manuscript received 5 February 1996; in final form 22 July 1996)

ABSTRACT

We present self-consistent comparisons of axissymmetric and 3-dimensional simulations of the tropospheric circulation under idealized physical conditions. These reveal a feedback of transient eddies onto the Hadley circulation which, first, strongly depends on equatorial heating and, second, is in case of realistic heating quite different from prescribed eddy forcing. A quantitative estimation for the eddy-induced mixing of vorticity into the poleward flow of the Hadley cell is given. The proposed relation is in accordance with observations. It is derived from the computational result that eddy momentum flux convergence is of the same order as the equatorward flux of relative vorticity generated by the Hadley circulation. Evaluation of the local budgets of sensible heat gives rise to a clear picture of how the poleward heat transports due to Hadley circulation and transient eddies interlock. This mechanism is found to be essential for an interpretation of the eddy feedback.

1. Introduction

Since the early work of Hadley, the tropospheric circulation has been subject to a variety of investigations. Lorenz (1967) has given a comprehensive review and discussed the general circulation in the time mean of the zonally averaged frame. The main features in this picture are a strong tropical Hadley cell driven by cumulus heating and large-scale midlatitude eddies driven by the overall equator to pole difference in diabatic heating. A comparison of the zonally averaged Hadley circulation with axissymmetric models was lacking.

Schneider (1977) first showed that a reasonable Hadley cell accompanied by a sharp subtropical wind jet can be simulated with an axissymmetric (herafter 2D) model. He also found that the zonal wind maximum was too large, indicating that eddies reduce rather than maintain the jet. Held and Hou (1980) found similar results based on an idealized 2D model, simulating diabatic processes by temperature relaxation, linear surface drag and globally constant turbulent viscosity only. They noticed that even though the Hadley cell intensity strongly decreases with decreasing viscosity, it remains final in the low viscous limit. Their analytical description of the quasi inviscid solution obtained in Boussinesq approximation and for symmetry with respect to the equator is known as the Held–Hou model (hereafter HHM) of the Hadley cell (James, 1994). The HHM is based on angular momentum and energy conservation within the meridional circulation. These assumptions are generally valid in quasi inviscid 2D dynamics. An open question of the HHM was that the circulation strength turned out to be only a little fraction of the observed annual mean.

Later on, Lindzen and Hou (1988) found that the meridional mass circulation increases rapidly when the heating maximum is centered off the equator. Thus the HHM has been brought more in accordance with observations. Remaining short-

* Corresponding author.

comings were suggested to be caused by the simplifications of the model, especially by the lack of cumulus heating known as the main energy source of the Hadley circulation. Accordingly, Hou and Lindzen (1992) proved that concentrated thermal forcing in the intertropical convergence zone, simulated in their numerical model by modifying the equilibrium temperature profile used for relaxation, improves the idealized 2D approach again.

Obviously, Hadley cell as well as zonal wind profile are extremely sensitive to position and intensity of equatorial heating. On the other hand, baroclinic instability strongly depends on the structure of the subtropical jet (Barnes and Young, 1992). Hence, one expects important correlations between equatorial heating anomalies and wave activity in extratropics. Such correlations have been investigated by Hou (1993), Chang (1995), Ulbrich et al. (1995) and many others. In view of the aforementioned 2D results it is most probable that these correlations correspond to the sensitivity of midlatitude waves to changes of the Hadley cell intensity (Lindzen, 1994).

Another question is how eddies influence the Hadley cell. Such an effect can be derived from observational or GCM data by diagnostic methods. These yield the alteration of the mean meridional circulation due to the meridional eddy flux convergences of angular momentum and sensible heat. A corresponding analysis has been done by Pfeffer (1981) for instance. According to Pfeffer's study, approximately 25% of the winter Hadley cell intensity is driven by eddies while the remainder is due to diabatic heating in deep tropics with rates of about 1–2 K/day. Results of Dethloff and Schmitz (1981) for annual mean data are similar to those of Pfeffer (1981) and also inidicate that eddy momentum flux causes reduction and poleward shift of the zonal wind jet. On the basis of these studies one is tempted to conclude that eddies amplify the Hadley circulation by a comparatively minor fraction. One would also expect that axissymmetric models are appropriate — apart from standing and travelling waves in the tropics.

In diagnostic models, diabatic heating and eddies are decoupled and prescribed; in dynamical models these quantities are coupled. Therefore the response of the Hadley circulation due to eddy forcing is not neccessarily identical with the difference between three dimensional (herafter 3D) and 2D dynamics. The difference between the time and zonally averaged and the axissymmetric tropical meridional circulation is rather the dynamical response due to inclusion of eddies or simply the eddy feedback.

The question of eddy feedback can be illuminated by comparisons of 2D and 3D simulations of the tropospheric circulation. Such comparisons are already possible from the studies of Williams (1988a and 1988b) and Satoh et al. (1995). These authors utilized comprehensive GCMs, including moisture and radiation processes. Their computations are similar with respect to the physical input but yield considerably different results in 2D dynamics. One must keep in mind that parametrizations of physical processes as implemented in available GCMs do often not allow consistent transformation of a 3D into a 2D model. We will point on the problem connected with horizontal diffusion in Section 2. As discussed by Satoh (1994), difficulties do also occur if some common cumulus convection schemes are used in a 2D model. This complexity of comprehensive GCMs renders interpretation of discrepancies more difficult.

Therefore, in the present study, we stay with an idealized model for dry air (hereafter SGCM) which ensures self-consistence of zonally averaged and axissymmetric results. For simplicity, longitudinally invariant model conditions are prescribed, excluding orographic effects and stationary waves. Following Hou (1993), we simulate the effects of radiation, latent heat release and convection via temperature relaxation towards a typical climate state and additional, prescribed cumulus heating Q_c in tropics. Alterations of the Hadley cell due to inclusion of eddies are investigated for different amplitudes of Q_c. The concepts of eddy forcing as well as angular momentum and energy conservation are discussed with respect to present results.

Fields according to axissymmetric modelling will be referred as "2D" fields while time and zonally averaged fields due to 3D computations will be referred to as "3D" fields. After describing the model (Section 2), we compare the climatologies of self-consistent 2D and 3D experiments for different equatorial heating rates (Section 3). Interpretations are drawn from the mass-weighted local budgets of angular momentum and sensible

heat (Section 4). In Section 5, some results are discussed in the context of previous studies. Finally, Section 6 gives a summary and some concluding remarks.

2. Description of the SGCM

The basis of the present investigation is a hybrid level circulation model with spherical geometry and spectral representation in horizontal direction. The applied methods are standard, i.e., vertical discretization according to Simmons and Burridge (1988), spectral transformation using Gaussian quadrature and Fourier transform (Machenhauer and Rasmussen, 1972) as well as semi-implicit time stepping (Asselin, 1972; Hoskins and Simmons, 1975). This section defines the basic equation system and specifies the model parameters.

Pressure p is represented as a function of vertical coordinate η and surface pressure p_s

$$p(\eta; p_s) = a(\eta) + b(\eta)p_s. \tag{1}$$

The coefficients a and b must guarantee monotonic growth of p with η as well as $p(\eta = 0; p_s) = 0$ and $p(\eta = 1; p_s) = p_s$. Usually the flexibility of (1) is used to let surfaces of constant η correspond to σ-levels near the ground and to pressure levels in the upper atmosphere. To achieve such a behaviour we define

$$a(\eta)/p_{ref} := \eta(1 - \eta) \quad \text{and} \quad b(\eta) := \eta^2 \tag{2}$$

with $p_{ref} \equiv 1013$ mb denoting the global mean surface pressure.

The prognostic primitive equations for horizontal vorticity ξ, horizontal divergence D, temperature T and surface pressure may be written as

$$\partial_t \xi = (\nabla \times \boldsymbol{F}) \cdot \boldsymbol{e}_z, \tag{3}$$

$$\partial_t D = \nabla \cdot \boldsymbol{F} - \nabla^2 \left(\frac{\boldsymbol{v}^2}{2} + \Phi \right), \tag{4}$$

$$\boldsymbol{F} := ((f + \xi)v - \dot{\eta}\partial_\eta u)\boldsymbol{e}_\lambda + (-(f + \xi)u - \dot{\eta}\partial_\eta v)\boldsymbol{e}_\phi - \frac{RT}{p}\nabla p + \boldsymbol{R}, \tag{5}$$

$$\mathrm{d}_t T = \frac{RT}{c_p p}\omega - \frac{T - T_e}{\tau} + Q_c + q + q_{diss}, \tag{6}$$

$$\partial_t p_s = -\int_0^1 \nabla \cdot (\partial_\eta p \boldsymbol{v})\, \mathrm{d}\eta. \tag{7}$$

Horizontal velocity field and horizontal ∇-operator are denoted by $\boldsymbol{v} = u\boldsymbol{e}_\lambda + v\boldsymbol{e}_\phi$ and $\nabla = (\boldsymbol{e}_\lambda/a_e \cos\phi)\partial_\lambda + (\boldsymbol{e}_\phi/a_e)\partial_\phi$. $\boldsymbol{e}_\lambda$, $\boldsymbol{e}_\phi$ and $\boldsymbol{e}_z$ are unit vectors in longitudinal, meridional and vertical direction, respectively. f is the Coriolis parameter and a_e the radius of the earth. R and c_p are molar gas constant and heat capacity of dry air. $\boldsymbol{F}$ contains all terms of the horizontal momentum equations that cannot be written as a gradient. $\boldsymbol{R} = R_u\boldsymbol{e}_\lambda + R_v\boldsymbol{e}_\phi$ describes friction due to vertical shear. The diabatic terms of the energy eq. (6) are temperature relaxation and constant equatorial heating (with prescribed fields $T_e(\phi, p)$ and $Q_c(\phi, p)$), vertical diffusion q and energy dissipation q_{diss} due to $\boldsymbol{R}$. A relaxation time of $\tau = 15$ days is used throughout this study.

The prognostic equations (3)–(7) are completed by (1), (2) and expressions for geopotential Φ, vertical velocity and pressure velocity ω:

$$\Phi = \Phi_s + \int_\eta^1 \frac{RT}{p}\frac{\partial p}{\partial \tilde{\eta}}\, \mathrm{d}\tilde{\eta}, \tag{8}$$

$$\dot{\eta} = \left(b \int_0^1 \nabla \cdot (\partial_\eta p \boldsymbol{v})\, \mathrm{d}\eta - \int_0^\eta \nabla \cdot (\partial_{\tilde{\eta}} p \boldsymbol{v})\, \mathrm{d}\tilde{\eta} \right) \Big/ \partial_\eta p, \tag{9}$$

$$\omega = b(\boldsymbol{v} \cdot \nabla)p_s - \int_0^\eta \nabla \cdot (\partial_{\tilde{\eta}} p \boldsymbol{v})\, \mathrm{d}\tilde{\eta}. \tag{10}$$

Eq. (8) follows from vertical integration of the hydrostatic approximation

$$\partial_\eta \Phi = -\frac{RT}{p}\partial_\eta p, \tag{11}$$

with Φ_s denoting the geopotential height of the orography which is omitted in the present investigation. Vertical velocity, pressure velocity and surface pressure tendency follow from integrations of the continuity equation

$$\partial_t(\partial_\eta p) + \nabla \cdot (\partial_\eta p \boldsymbol{v}) + \partial_\eta(\partial_\eta p \dot{\eta}) = 0, \tag{12}$$

with respect to the kinematic boundary condition

$$\dot{\eta} = 0 \quad \text{for } \eta = 0 \quad \text{and } \eta = 1. \tag{13}$$

For simplicity, we use the height z to define vertical diffusion:

$$\begin{Bmatrix} \boldsymbol{R} \\ q \end{Bmatrix} = \frac{1}{\rho}\partial_z \begin{Bmatrix} \rho\nu\partial_z \boldsymbol{v} \\ \rho\nu\partial_z \Theta \end{Bmatrix}. \tag{14}$$

In (14), $\rho = p/RT$ and $\Theta = T(p_{ref}/p)^{\kappa}$ denote density and potential temperature with $\kappa := R/c_p$. ν plays the role of a turbulent viscosity. Dissipation per unit mass due to $\boldsymbol{R}$ is given by $\nu(\partial_z \boldsymbol{v})^2$, yielding

$$q_{diss} = \nu(\partial_z \boldsymbol{v})^2/c_p, \tag{15}$$

We apply dynamic boundary conditions of the form

$$\nu\partial_z \boldsymbol{v} = c_v \boldsymbol{v}_1 \quad \text{and} \quad \nu\partial_z \Theta = c_\Theta(\Theta_1 - \Theta_s) \quad \text{for } z = 0, \tag{16}$$

which balance the lower boundary wind stress with the wind in the lowest layer (indicated by the index 1) and the lower boundary heat flux with the corresponding temperature deviation from a prescribed surface temperature Θ_s defined as $T_e(\varnothing, p_s)(p_s/p_{ref})^{\kappa}$.

The coefficients ν, c_v and c_Θ are specified according to 2 parametrizations. The first one is the local vertical diffusion scheme briefly described by Holtslag and Boville (1993). It is applied in the present study with minor modifications:

$$\nu := \left(\frac{1}{kz} + \frac{1}{30\text{ m}}\right)^{-2} |\partial_z \boldsymbol{v}| F(\mathrm{Ri}),$$

$$\mathrm{Ri} := \frac{g\partial_z \Theta}{\Theta(\partial_z \boldsymbol{v})^2},$$

$$F(\mathrm{Ri}) := \begin{cases} \sqrt{1 - 18\ \mathrm{Ri}} & \mathrm{Ri} < 0 \\ (1 + 9\ \mathrm{Ri} + 50\ \mathrm{Ri}^2)^{-1} & \mathrm{Ri} \geqslant 0, \end{cases}$$

$$c_v \equiv c_\Theta = c_N F_0(\mathrm{Ri}_0)|\boldsymbol{v}_1|, \tag{17}$$

$$c_N := \left(\frac{k}{\ln((z_1 + z_0)/z_0)}\right)^2,$$

$$\mathrm{Ri}_0 := \frac{g z_1(\Theta_1 - \Theta_s)}{\Theta_1 \boldsymbol{v}_1^2},$$

$$F_0(\mathrm{Ri}_0) := \begin{cases} F(\mathrm{Ri}_0) & \mathrm{Ri}_0 < 0 \\ 1 - 9\ \mathrm{Ri}_0/(1 + 75 c_N \\ \times \sqrt{|\mathrm{Ri}_0|(z_1 + z_0)/z_0)} & \mathrm{Ri}_0 \geqslant 0. \end{cases}$$

In (17), $k = 0.4$ denotes the van Kármán constant. z_1 is the height of the lowest model layer and the roughness length z_0 is set to 10^{-4} m. We will refer to (17) as the realistic vertical diffusion scheme. A second, idealized scheme can be chosen to ensure correspondence to numerical calculations of Held and Hou (1980) or Lindzen and Hou (1988). In the idealized scheme, ν is globally constant and $c_v = 0.005$ m/s as well as $c_\Theta = 0$ are fixed. All major computations presented in this study were performed with the more realistic vertical diffusion scheme (17). Only the case study presented in Fig. 11 (Section 5) is based on the idealized scheme.

Height-independent horizontal diffusion is applied equally to vorticity, divergence and temperature. Such additional damping terms are necessary (at least in 3D) to simulate turbulent dissipation at small scales. For total wavenumber n the damping rate is defined by the respective spectral amplitude times a scale selective factor L_n.

It should be noted that any horizontal diffusion in the primitive equations corresponds to an asymmetric stress tensor and therefore violates the basic laws of energy, momentum and angular momentum conservation. For example, an ordinary ∇^4-diffusion ($L_n \propto (n(n+1))^2$) is appropriate in 3D computations. In contrast, 2D dynamics of an idealized GCM is characterized by a stationary solution, and even the weakest ∇^4-diffusion destroys the basic balance requirements.

To allow for self-consistent 2D and 3D dynamics we must utilize a horizontal diffusion scheme which fullfills two conditions: It must behave nearly neutral in 2D computations, but nevertheless it should simulate dissipation at small scales in the presence of waves. The scheme

$$L_n = \begin{cases} k(n - n_*)^2 & \text{for } n > n_* \\ 0 & \text{otherwise} \end{cases} \tag{18}$$

proposed by Laursen and Eliassen (1989) has been found to satisfy these conditions. For standard T21 spectral resolution we choose $n_* = 15$ and k such that total wavenumber 21 is damped with one day.

We use a vertical resolution of 15 unequally spaced hybrid levels. For $p_s = p_{ref}$ full pressure levels in mb are given from top to ground by: 23.0, 72.2, 128.2, 191.5, 262.0, 339.1, 421.4, 506.5, 591.6, 673.9, 751.0, 821.5, 884.8, 940.8, 990.0.

Equilibrium temperature T_e and distribution of additional equatorial heating Q_c are depicted in Fig. 1. These axissymmetric fields are used for the major computations presented in this study. They are given by analytical formulas. Calculation of T_e is described in the appendix while Q_c is defined

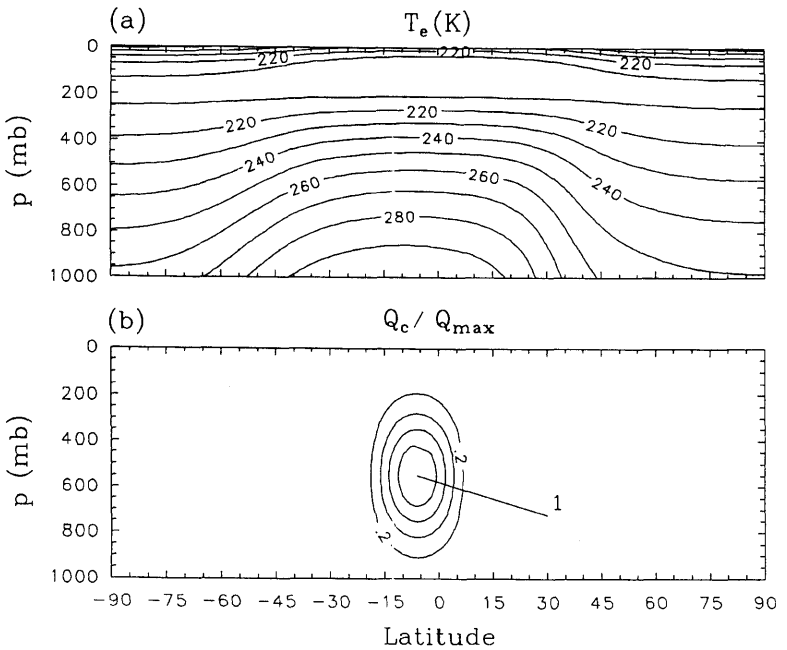

Fig. 1. Fields for simulation of thermal forcing. (a) Equilibrium temperature T_e (contour interval 10 K). The parameters of T_e are: $\varnothing_{eq} = -10°$, $p_{bo} = 1013$ mb, $p_{tr} = 110$ mb, $p_{to} = 10$ mb, $T_{eq} = 300$ K, $T_{po} = 255$ K, $T_{tr} = 200$ K, $T_{to} = 220$ K, $\varnothing_{je} = 40^0$, $s_\varnothing = 0.55$, $p_{je} = 200$ mb, $s_p = 210$ mb. (b) Additional equatorial heating Q_c/Q_{max} (contour interval 0.2). The parameters of Q_c are: $p_0 = 550$ mb, $\sigma_p = 200$ mb, $\varnothing_0 = -6°$, $\sigma_\varnothing = 18°$.

by

$$Q_c(\varnothing, p; Q_{max}, p_0, \sigma_p, \varnothing_0, \sigma_\varnothing)/Q_{max} = \begin{cases} \exp\{-(p-p_0)^2/(2\sigma_p^2)\} \\ \times \cos^2\{(\pi/2)(\varnothing - \varnothing_0)/\sigma_\varnothing\} & \text{for } |\varnothing - \varnothing_0| < \sigma_\varnothing \\ 0 & \text{otherwise.} \end{cases} \quad (19)$$

To perform the case study presented in Fig. 11, T_e is varied with respect to its asymmetry parameter $\varnothing_{eq}$ (see Appendix). $T_e(\varnothing, p; \varnothing_{eq} = 0)$ is also used as initial temperature for model integrations. The corresponding intial wind u_e is calculated from the general thermal wind relation such that (T_e, u_e) is a stationary solution of the adiabatic equation system. Under the influence of the diabatic processes, (T_e, u_e) changes into the stationary solution of the 2D model. If in addition the initial condition is disturbed by wave excitation, a mean climate state is obtained with the 3D model after a few months of integration. Time averaging of 3D results is done using 180 days intervals with a sampling rate of 12 h. Because the asymptotic 2D solution shows slight oscillations in the low viscous range, we generally present time averaged results also in the 2D case, using 5-year intervals with a sampling rate of 10 days.

3. 2D versus 3D: model climatologies

3.1. *Weak equatorial heating*

Figs. 2a, b show the meridional mass streamfunctions obtained in 2D and 3D for $Q_c = 0$. This case corresponds to the model setup of Held and Hou (1980) or Lindzen and Hou (1988) (apart from the vertical diffusion scheme and the equation of state). In the winter hemisphere both 2D and 3D computation exhibit a direct meridional circulation confined to the tropics. The 3D run reveals (in addition to Ferrel and a weak polar cell) a 6 times amplification of the Hadley cell (note the different contour intervals). Maxima of

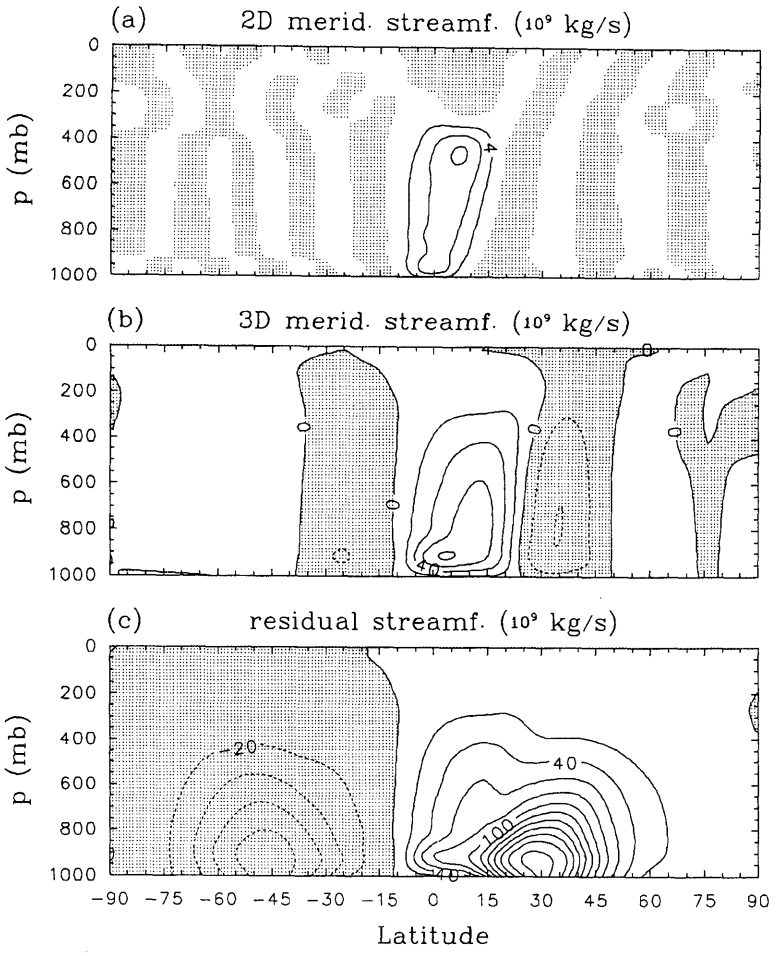

Fig. 2. Comparison of (a) 2D, (b) 3D Eulerian and (c) 3D residual meridional mass streamfunction in case of $Q_c = 0$. Contour intervals are 4, 20 and 20×10^9 kg/s, respectively. Streamfunction maxima in (a) and (b) are 13 and 83×10^9 kg/s. Shaded areas indicate negative values.

the streamfunctions are 13 and 83×10^9 kg/s, respectively. The residual circulation (Fig. 2c) has been computed according to Edmon et al. (1980), using eq. (3.4) in their paper. Residual and Eulerian streamfunction are nearly identical in deep tropics, suggesting that the 2D → 3D intensification of the Hadley cell corresponds to an intensification of the residual circulation.

According to the analysis of Pfeffer (1981), realistic eddy fluxes account for approximately 50×10^9 kg/s of the winter Hadley cell intensity. Using this result to interpret the 2D → 3D intensification, one must note that in the present 3D computation, subtropical eddy flux convergences (not shown) reach about only half of realistic amplitudes. Therefore the 2D → 3D amplification of the Hadley cell can at most partly be interpreted as a response to prescribed eddy forcing. In Section 4.2 we will show that diabatic heating in deep tropics has strongly increased from 2D to 3D.

3.2. *Realistic equatorial heating*

A simple general circulation model without additional (or concentration in) equatorial heating fails to generate a Hadley cell which is realistic with respect to intensity and altitude of the streamfunction maximum. The reason is the lack of

cumulus convection which in reality results in a heating maximum of about 1–2 K/day in the upper region (~ 550 mb) of the intertropical convergence zone. Therefore cumulus heating is simulated by adding Q_c to the right side of the thermodynamic equation (6). Note that diabatic heating remains a dynamic quantity because relaxation towards T_e plus Q_c corresponds to relaxation towards $T_e + \tau Q_c$.

While raising the amplitude Q_{max} of Q_c, one finds that both the 2D and the 3D Hadley cell maximum rise in strength and altitude. The intensification is much more pronounced in 2D. A realistic maximum of the 3D meridional streamfunction of about 190×10^9 kg/s is achieved for $Q_{max} = 2.0$ K/day for instance. Fig. 3 shows corresponding 2D and 3D results. 3D meridional and residual streamfunction now crudely resemble observations. In contrast, the 2D model overestimates the tropical mass circulation by a factor of about two. (The maxima in Fig. 3a, b are 360 and 190×10^9 kg/s, respectively.) However, the streamfunction maximum is not the only property to consider. Comparison of the spatial structures of 2D and 3D Hadley cell yields that the eddies not only cause a reduction of the mass circulation in the upper troposphere but also a strong intensification of the equatorward flow below. Such a behaviour is quite different from eddy forcing: The diagnostic model would predict that in absence of eddies the streamfunction maximum is weaker by about 50×10^9 kg/s and that the response is concentrated at high altitudes (see Fig. 6 in Pfeffer (1981)).

Fig. 4 shows the mean zonal winds. In the winter hemisphere both computations exhibit a sharp subtropical wind jet. The 2D jet core is located at the edge of the Hadley cell due to angular momentum conservation of overturning air parcels. In comparison, the 3D jet is reduced, broadened and shifted. About such an effect has been speculated by Lindzen and Hou (1988) as a result of eddy induced angular momentum reduction in the poleward flow of the Hadley cell. The 2D computation yields double maxima of the zonal wind jet which is more pronounced in the summer hemisphere. Such an effect has also been found by Held and Hou (1980) in the quasi inviscid limit or by Hou and Lindzen (1992) in case of concentrated equatorial heating. In the presence of waves the wind maxima merge due to the poleward shift of the equatorward one.

4. 2D versus 3D: local budgets

As a first step in understanding the 2D→3D alterations of tropical dynamics we study the terms that contribute to the equations of motion. Let us consider the zonally averaged forms of the zonal wind equation and the first law in pressure coordinates:

$$\partial_t \bar{u} = (\bar{\xi} + f)\bar{v} - \bar{\omega}\partial_p \bar{u} + \bar{R}_u + \mathrm{conv}(u'v') - \partial_p(\overline{u'\omega'}), \tag{20}$$

$$\partial_t \bar{T} = -\bar{v}\frac{\partial_\phi}{a_e}\bar{T} + a(s) + \bar{Q} + \mathrm{conv}(T'v', T'\omega'). \tag{21}$$

The bars denote zonal mean values while eddies are marked by primes. Q represents the sum of temperature relaxation, additional equatorial heating, vertical diffusion and dissipation. For simplicity we have introduced the abbreviations

$$\mathrm{conv}(u'v') := -\frac{\partial_\phi}{a_e \cos^2\phi}(\cos^2\phi\,\overline{u'v'}), \tag{22}$$

$$\mathrm{conv}(T'v', T'\omega') := -\frac{\partial_\phi}{a_e \cos\phi}(\cos\phi\,\overline{T'v'}) - \partial_p(\overline{T'\omega'}) + \frac{R}{c_p p}\overline{T'\omega'}, \tag{23}$$

for meridional convergence of eddy momentum flux and total convergence of eddy heat flux. Furthermore we have defined

$$a(s) := -\frac{1}{c_p}\bar{\omega}\overline{T\partial_p s} \equiv -\bar{\omega}\partial_p\bar{T} + \frac{R}{c_p p}\overline{T\omega}. \tag{24}$$

In (24), s denotes the entropy per unit mass and $c_p a(s)$ represents the zonal mean change of sensible heat due to vertical advection of s by the mean meridional circulation.

The angular momentum budget of the Hadley cell is affected by conv$(u'v')$ as shown by Held and Phillips (1990) in case of forced Rossby waves in a shallow-water model. Here we are concerned with nonlineary coupled baroclinic waves and ask to what extent the wave flux convergences, and especially conv$(T'v', T'\omega')$, are consistent with both assumptions of the HHM, namely angular

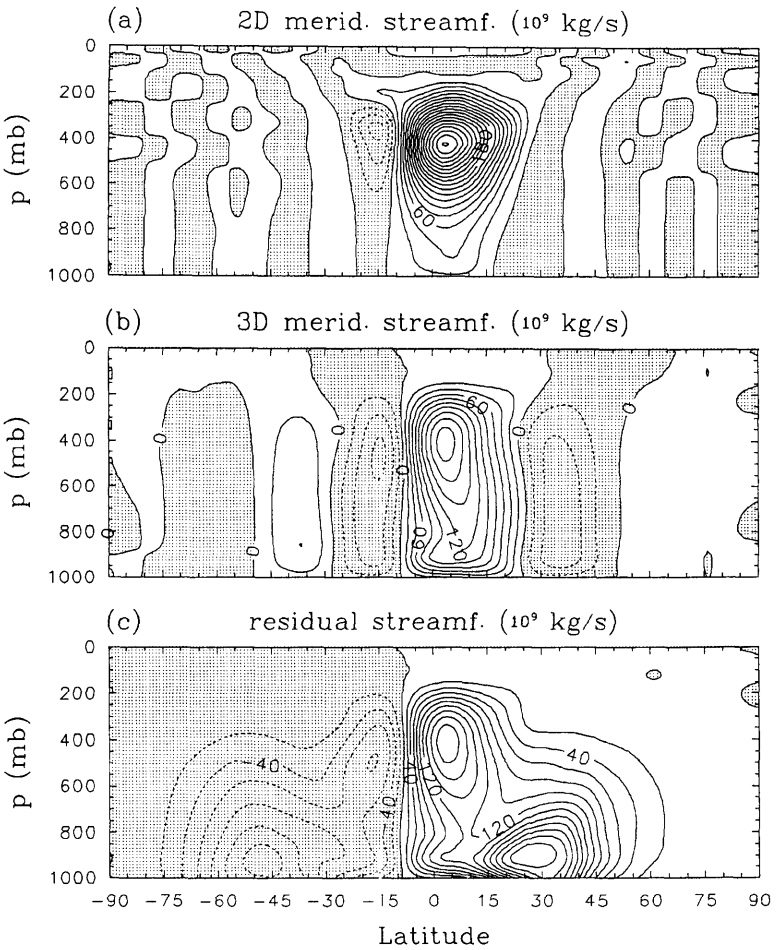

Fig. 3. Comparison of (a) 2D, (b) 3D Eulerian and (c) 3D residual meridional mass streamfunction in case of $Q_{max} = 2$ K/day. The contour interval is 20×10^9 kg/s. Streamfunction maxima in (a) and (b) are 360 and 190×10^9 kg/s. Shaded areas indicate negative values.

momentum and energy conservation of the Hadley circulation.

4.1. *Angular momentum budgets and vorticity mixing*

Figs. 5, 6 show the time means of the most important terms of (20) for the model runs with $Q_{max} = 2$ K/day. Let us consider the middle and upper troposphere of the tropics. First we recognize that the 2D results (Fig. 5) are in accordance with the HHM, i.e. in the region of the winter Hadley cell the Coriolis force $f\bar{v}$ is balanced by meridional transport $\bar{\xi}\bar{v}$ of relative vorticity. In other words, the absolute vorticity is approximately zero and we have

$$\bar{\xi} \approx -f \quad \text{in 2D.} \tag{25}$$

The situation is quite different in 3D (Fig. 6) where $f\bar{v}$ is balanced by similar amounts of $\bar{\xi}\bar{v}$ and $\text{conv}(u'v')$, i.e., in the poleward flow of the Hadley cell we have

$$\text{conv}(u'v') \approx \bar{\xi}\bar{v}. \tag{26}$$

With respect to the approximate time averaged form of (20)

$$f\bar{v} + \bar{\xi}\bar{v} + \text{conv}(u'v') \approx 0, \tag{27}$$

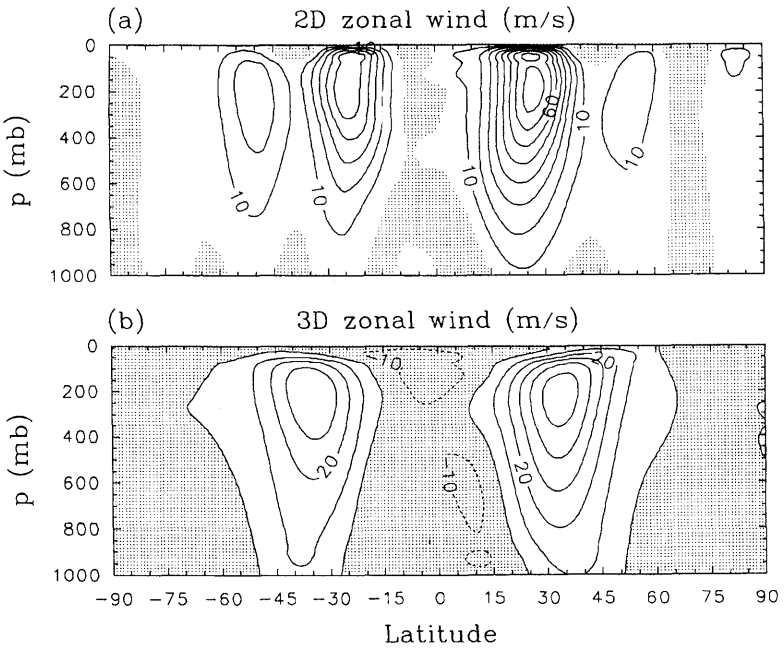

Fig. 4. Comparison of (a) 2D and (b) 3D mean zonal wind in case of $Q_{max} = 2$ K/day. The contour interval is 10 m/s. Shaded areas indicate negative values.

one can estimate the modification of (25) due to wave activity:

$$\bar{\xi} \approx -f/2 \qquad \text{in 3D.} \tag{28}$$

In Fig. 7, (28) is compared with model results and observational data for southern winter (from ECMWF analysis, July 1984–93). We did not use the data for northern winter in order to reduce the influence of stationary waves. The zonally and time averaged relative vorticity is plotted at 200 mb between $-20°$ and 30°. The observational data are plotted with negative sign and reversed latitude to ensure correspondence to the model. The mixing of absolute vorticity into the tropics is approximately described by the model run with realistic equatorial heating. Between 5° and 20° the empirical formula (28) gives a rough estimation of the situation in the winter Hadley cell. This holds as a first approximation also for the simulations with $Q_{max} = 0$ and 1 K/day. But Fig. 7 also indicates that vorticity mixing decreases if tropical heating increases.

Let us return to Figs. 5, 6 and consider the angular momentum budgets in midlatitudes. Here fv is small for the 2D run, i.e., there is no worth mentioning meridional circulation out of the Hadley cell and this is consistent with the construction of the HHM. In 3D, $f\bar{v}$ is approximately balanced by conv($u'v'$) as expected. In the lowest layers the Coriolis term is generally balanced by $\bar{R}_u$ which is not shown here.

4.2. *Heat budgets*

In Figs. 8, 9 the most important terms of the heat budget (21) are depicted for the model runs with $Q_{max} = 2$ K/day. In deep tropics, $a(s)$ is balanced by diabatic heating in 2D and 3D. Furthermore, entropy is advected in the downward flow of the Hadley cell. But here the 3D energy budget differs qualitatively from 2D where balance is achieved solely by diabatic cooling and backward horizontal advection.

In 3D (Fig. 9), subtropical cooling due to conv($T'v'$, $T'\omega'$) exceeds that due to $\bar{Q}$. In the lowest layers $\bar{Q}$ becomes positive. But this is not only caused by the minimum of conv($T'v'$, $T'\omega'$). Also equatorward advection of heat (not shown) gives an important contribution close to the boundary, reducing the effective $\bar{Q}$. Out of the

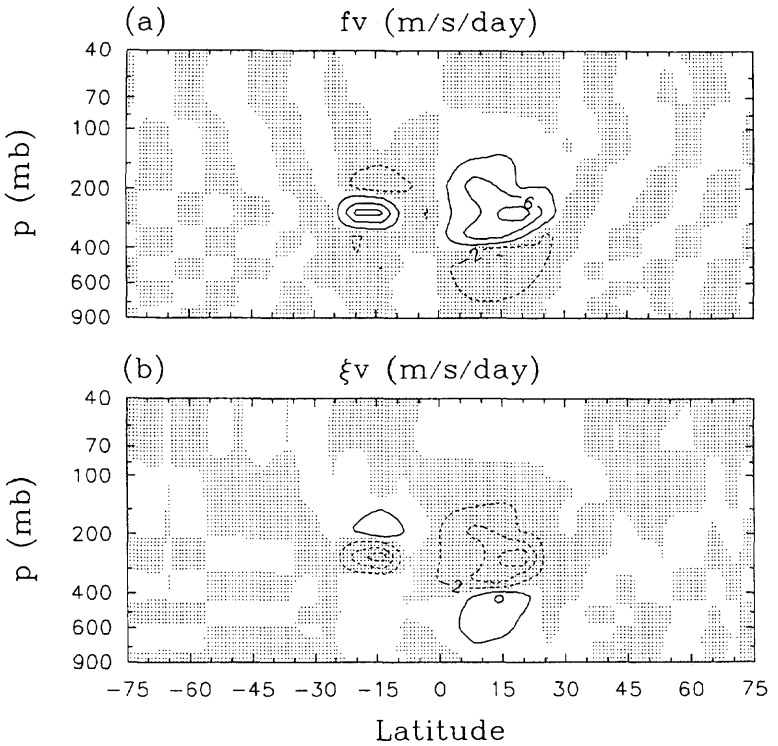

Fig. 5. Contributions to the 2D angular momentum budget in case of $Q_{max} = 2$ K/day: (a) $f\bar{v}$, (b) $\bar{\xi}\bar{v}$. The contour interval is 4 m/s/day. Shaded areas indicate negative values.

boundary layer, subtropical cooling due to conv($T'v'$, $T'\omega'$) is definitely balanced by entropy advection of descending zonal mean flow. This interpretation holds because $a(s)$ is the only positive contribution to the heat budget in that region. The mechanism has been found to be general in all our 3D simulations, independent from Q_{max}, ϕ_{eq} or the vertical diffusion scheme.

The total northward energy flux is given by the time mean of

$$\frac{a_e \cos \phi}{g} \int_0^{2\pi} d\lambda \int_0^{p_{ref}} dp\, v(c_p T + \Phi + \boldsymbol{v}^2/2). \qquad (29)$$

Inside the winter Hadley cell, this quantity is positive because the net poleward flux of potential energy exceeds the net equatorward flux of sensible heat. (The contribution of kinetic energy is negligible.) Therefore (29) increases in case of vertical elongation of the Hadley cell. Fig. 10 shows 2D and 3D total energy fluxes for $Q_{max} = 0$, 1 and 2 K/day. The effective Hadley cell intensities, i.e. the overall diabatic heating in deep tropics, can be measured by the energy fluxes at about 5 degrees north, indicated by vertical solid lines in Fig. 10. This latitude approximately marks the streamfunction maxima. (The 3D energy flux increases northward of 5 degrees due to diabatic heating in the low altitude equatorward flow.) Fig. 10a reveals a striking 2D → 3D intensification of deep tropical heating in case of $Q_c = 0$. The effective 2D → 3D intensification decreases with increasing amplitude of Q_c. An intensification remains even for maximum Q_c. This is consistent with the heating rates in Figs. 8a, 9a where deep tropical heating is slightly stronger in 3D. It is nevertheless consistent with Fig. 3 even though a strong 2D → 3D reduction of the streamfunction maximum shows up:

In 3D dynamics, the meridional circulation generally increases at low altitudes. This is indicated in Figs. 2, 3 by concentration of streamlines close to the lower boundary. It follows that the

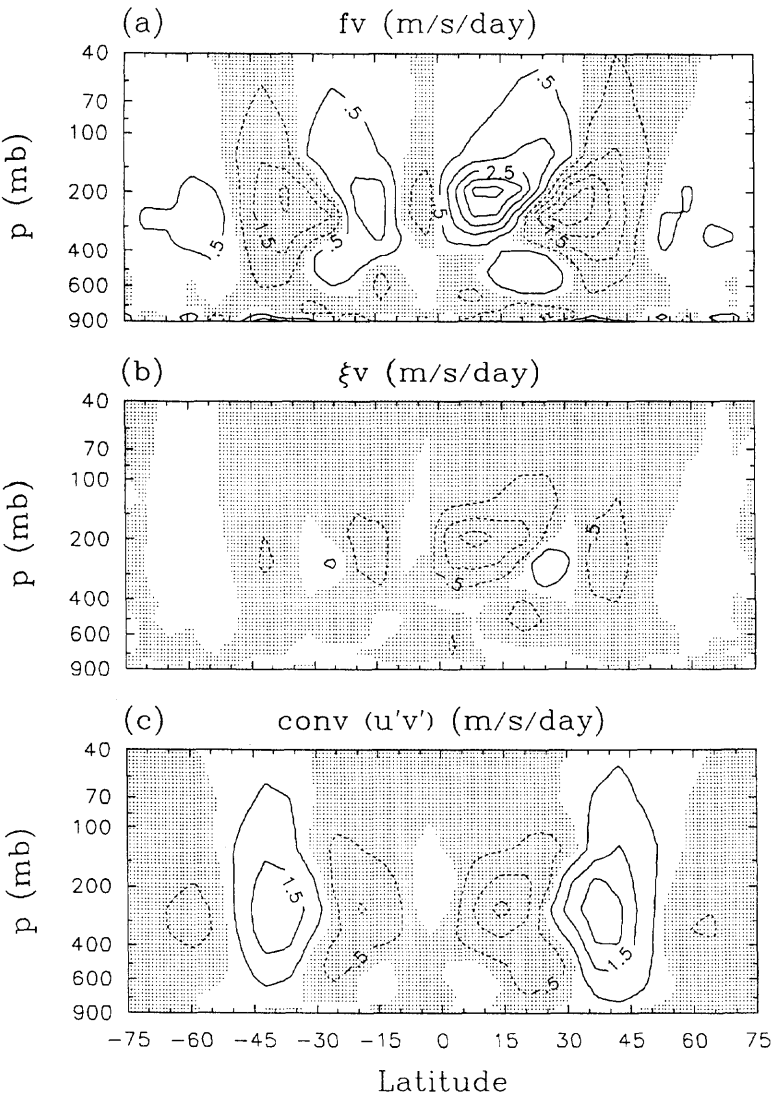

Fig. 6. Contributions to the 3D angular momentum budget in case of $Q_{max} = 2$ K/day: (a) $f\bar{v}$, (b) $\bar{\xi}\bar{v}$, (c) conv$(u'v')$. The contour interval is 1 m/s/day. Shaded areas indicate negative values.

total energy flux (29) generated by the Hadley circulation (mainly the flux of potential energy) strongly increases from 2D to 3D if no reduction of the high altitude streamfunction maximum occurs (which is the case for $Q_c = 0$). The two effects, namely low altitude intensification (or vertical elongation) and high altitude reduction tend to vanish out for additional equatorial heating. The first effect still dominates the latter even in the realistic case (Fig. 10c).

Summarizing, in the free atmosphere the heat budgets of the Hadley cell can approximately be written as

$$\bar{Q} + a(s) - \bar{v}\frac{\partial_\sigma}{a_e}\bar{T} \approx 0 \qquad \text{in 2D,} \tag{30}$$

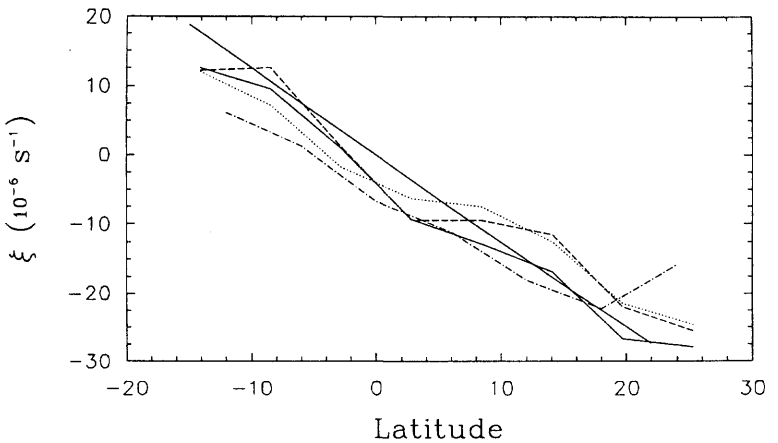

Fig. 7. Time and zonally averaged relative vorticity in the 200 mb layer. Computational 3D results are shown for $Q_{max} = 2$ K/day (solid line), $Q_{max} = 1$ K/day (dashed line) and $Q_c = 0$ (dotted line). Data from ECMWF analysis for southern winter (July 1984–93; dashed and dotted line) are plotted with negative sign and reversed latitude. The mixing relation (28) is indicated by an additional straight solid line.

$$\bar{Q} + a(s) + \mathrm{conv}(T'v', T'\omega') \approx 0 \qquad \text{in 3D,} \qquad (31)$$

where horizontal advection or eddy heat flux convergence are relevant only in subtropics.

5. Discussion

Computations with $Q_c = 0$ have also been performed with globally constant turbulent viscosity ν and linear wind stress condition as well as zero heat flux at the lower boundary (see Section 2). This model setup ensures that corresponding experiments are closely related to those of Held and Hou (1980) or Lindzen and Hou (1988). Figs. 11a, 11b summarize the results by showing the streamfunction maximum according to 2D and 3D modelling as functions of the asymmetry parameter $\varnothing_{eq}$ of T_e and viscosity ν. In addition, Fig. 11c shows the 2D → 3D amplification of the respective Hadley cells maxima.

According to Fig. 11a, the 2D Hadley cell strongly increases with increasing viscosity or asymmetry which reflects results of Held and Hou (1980) and Lindzen and Hou (1988). The quasi inviscid limit is indicated in the left lower corner by vertical alignment of contours. For decreasing viscosity the present 2D results also showed (like in Held and Hou (1980)) a rising in altitude of the Hadley cell maximum. The 2D → 3D intensification (Fig. 11c) is strongest in the low viscid limit where the 2D Hadley cell is driven solely by diabatic heating rather than by internal friction. The amplification exceeds values of 40 for symmetry with respect to the equator and is larger than 2 for all parameters used here. Results of a 2D–3D comparison in case of weak equatorial heating have also been mentioned by Saravan (1993) who used a two layer model with equator-symmetric conditions. He found an amplification factor of 5 which fits to Fig. 3c.

The 3D Hadley cell (Fig. 11b) is nearly independent from ν as long as $\nu \leqslant 1$ m^2/s. This indicates that in 3D the quasi inviscid limit is approached faster than in 2D. Comparison of Figs. 11a, b with Figs. 2a, b also suggests that the realistic vertical diffusion scheme (17) corresponds to the low viscous range of the idealized scheme. (Note that the 2D winter Hadley cell computed with (17) is even weaker than that obtained for $\nu = 0.1$ m^2/s.) For high values of ν, the 3D Hadley cell becomes stronger while eddy activity and Ferrel cell (both not shown) become weaker. The 3D Hadley cell reaches realistic intensities in case of high viscosity but concentrates its mass circulation at low altitudes which is not realistic. Hence, the quasi inviscid limit in connection with additional equatorial heating ensures correspondence to observations rather than the high viscous range with $Q_c = 0$.

It is remarkable that the HHM (as described in

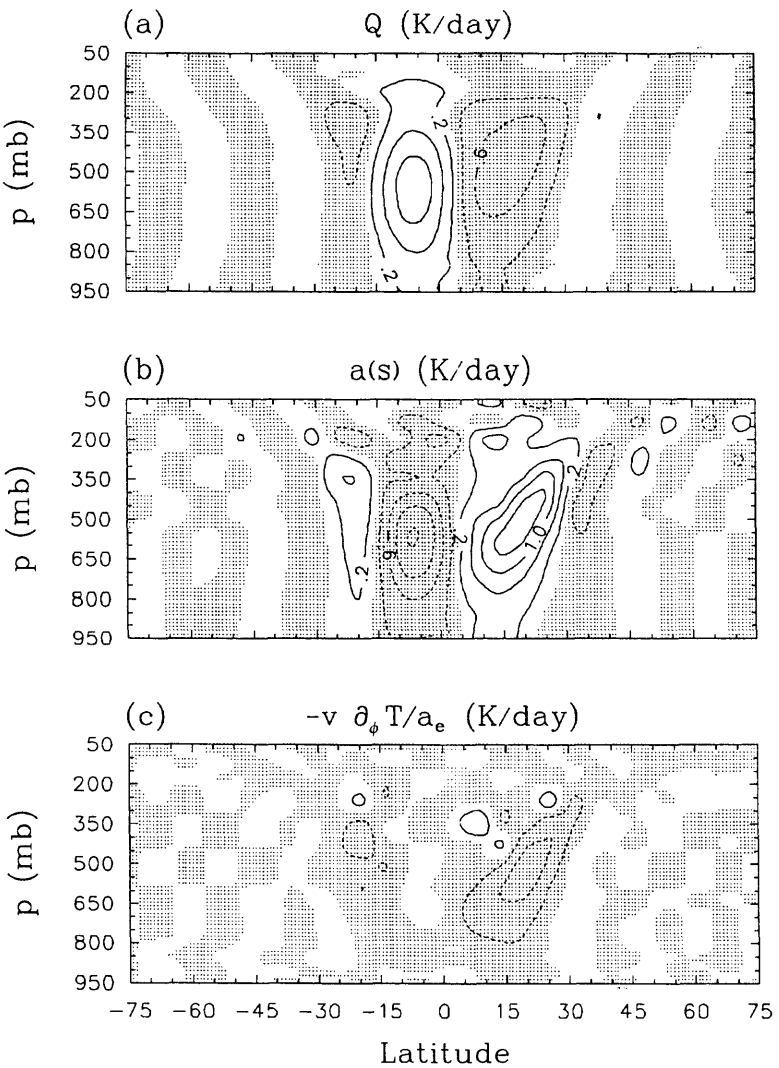

Fig. 8. Contributions to the 2D heat budget in case of $Q_{max} = 2$ K/day: (a) diabatic heating, (b) vertical advection and (c) horizontal advection. The contour interval is 0.4 K/day. Shaded areas indicate negative values.

James, 1994, for instance) predicts a stronger Hadley cell due to vorticity mixing. Let us stay with the assumption that the zonal wind increases lineary with height by a rate proportional to the high level relative vorticity. If we assume (28) instead of (25) as starting point of the HHM, the zonal wind is halfened inside the entire Hadley cell. In turn, the thermal wind relation predicts that the meridional temperature gradient also decreases by a factor of 2. Finally, energy conservation can only be fullfilled by larger temperature deviations from the prescribed equilibrium temperature. At the equator the HHM predicts doubling of diabatic heating. Because (28) is a much better description of the 3D angular momentum budget than (25), the simple analytical formulas of the HHM give at least a qualitative explanation of the 2D→3D Hadley cell intensification in case of $Q_c = 0$. The situation is more complex if additional equatorial heating is involved. Here a

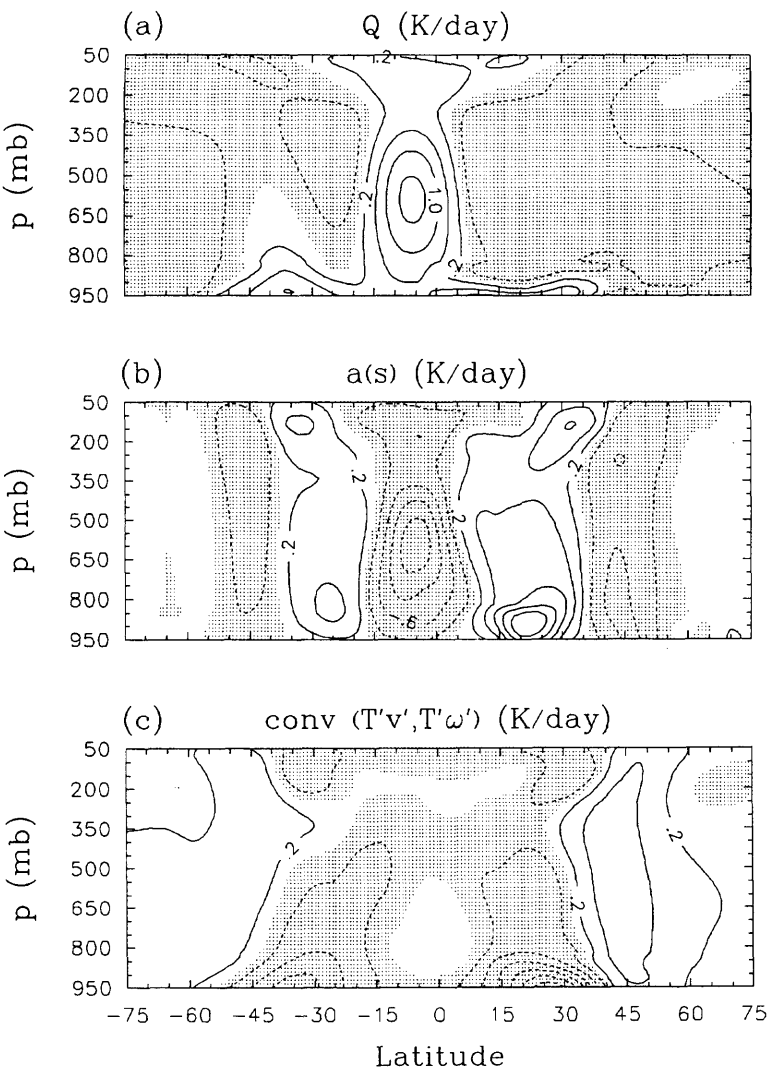

Fig. 9. Contributions to the 3D heat budget in case of $Q_{max} = 2$ K/day: (a) diabatic heating, (b) vertical advection and (c) eddy heat flux convergence. The contour interval is 0.4 K/day. Shaded areas indicate negative values.

latitudinal dependency of $\sin^2 \phi$ for the effective equilibrium temperature in the HHM seems to be less appropriate. Furthermore, as outlined in Subection 4.2, energy conservation of the 3D Hadley circulation can only be fullfilled with the inclusion of eddies.

Our major 3D results for $Q_{max} = 0$ and $Q_{max} = 2$ K/day are closely related to the control and standard perturbation experiment performed by Chang (1995). In spite of the various differences between the present model and that used by Chang, the computations are in good agreement. Especially, we have also found (but not shown here) an equatorward shift of the 3D zonal wind maximum due to enhanced equatorial heating, both in the northern and the southern hemisphere. This shift fits well to Fig. 7 which shows decreasing vorticity mixing (or increasing angular momentum conservation) for increasing equatorial heating. Furthermore, it follows from fig.10 that the 3D

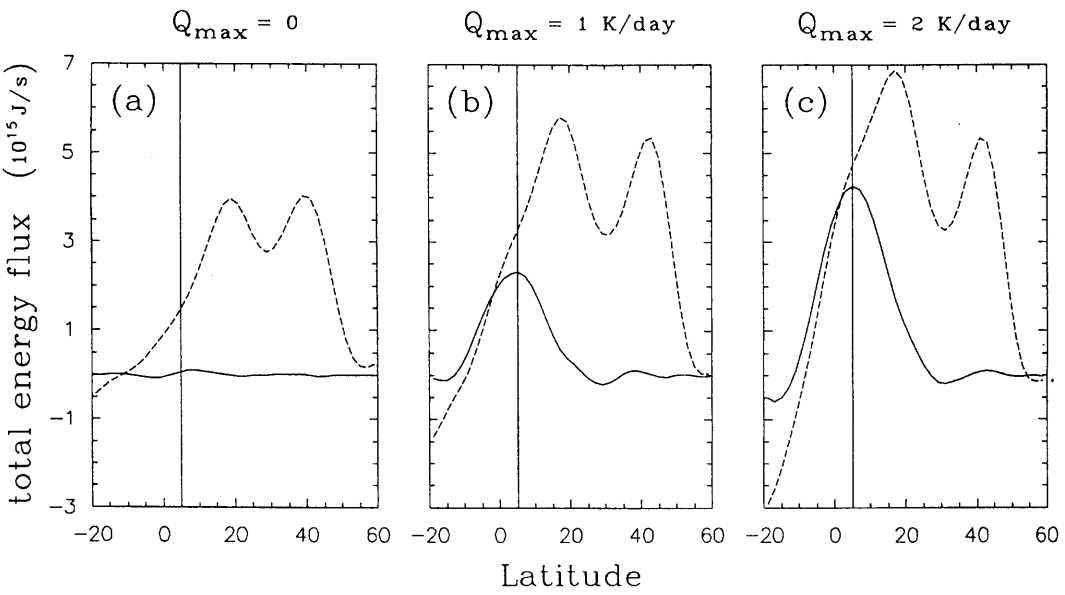

Fig. 10. Northward flux (29) of total energy in 10^{-15} J/s according to 2D (solid lines) and 3D (dashed lines) dynamics: (a) $Q_c = 0$, (b) $Q_{max} = 1$ K/day and (c) $Q_{max} = 2$ K/day. The approximate latitude of the Hadley cell maxima is indicated by vertical lines at 5° north.

midlatitude energy flux increases from $Q_c = 0$ to $Q_c > 0$. This is also in accordance with the results of of Chang (1995).

As mentioned in Section 1, a 2D–3D comparison has been done by Satow et al.(1995). The Hadley cells found by the authors are characterized by a broad 2D circulation at high altitudes and a strong 2D→3D intensification of the low altitude equatorward flow. Corresponding zonal wind jets clearly show reduction and poleward shift from 2D to 3D dynamics. These 2D→3D alterations are also visible in Figs. 3, 4.

Another 2D–3D comparison is possible from the studies of Williams (1988a and 1988b). He performed numerical computations similar to those of Satoh et al.(1995). Williams discussed that his 2D meridional circulation bears little resemblance with a typical Hadley cell (see Fig. 2 in Williams, 1988b). Furthermore, his 2D→3D alteration of the zonal wind maximum seems to indicate an equatorward shift of the tropospheric jet (compare Fig. 1c in Williams, 1988b with Fig. 2d in Williams, 1988a). This behaviour is quite opposite to our results or those of Satoh et al. (1995). We speculate that the discrepancies are related to the numerical details of the models.

It has been proven that vertical diffusion of heat (including surface heat flux) has little influence on the overall results presented in this study. A weak model response to neglection of heat diffusion is only found in 3D for temperature and local heat budget. The response is such that the lack in heating due to diffusion is partly compensated by enhanced heating due to relaxation but in the main by pronounced vertical advection $a(s)$ in subtropics. Thus the heat transfer mechanism described in Section 4.2 becomes even more obvious when diffusion of heat is switched off.

6. Summary and conclusions

For varying equatorial heating rates Q_c we have compared equivalent 2D and 3D SGCM simulations. It has been shown that transient midlatitude waves always have important impacts on the Hadley circulation which cannot generally be interpreted with prescribed eddy forcing, especially not in case of realistic equatorial heating. This seems not surprising: Eddy momentum flux convergence for instance strongly depends on the Hadley cell intensity in a dynamical model (Held

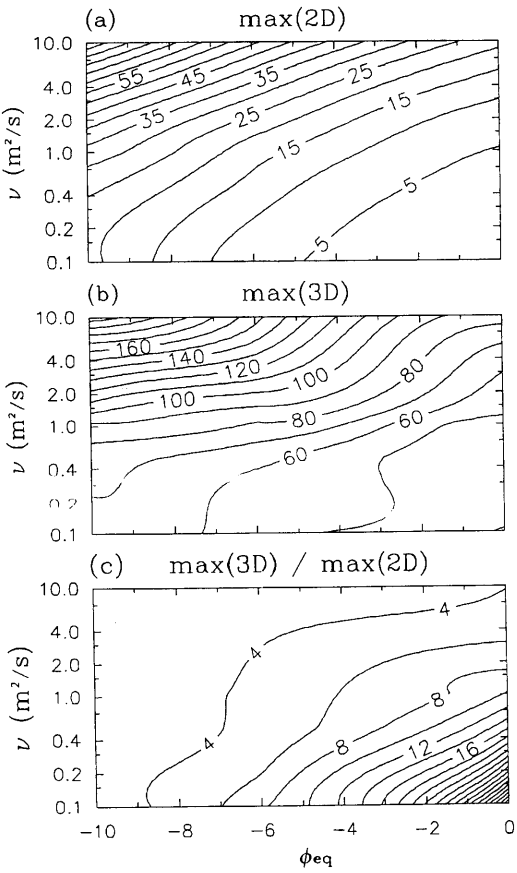

Fig. 11. Maxima of 2D (a) and 3D (b) meridional mass streamfunction as well as the corresponding 2D → 3D amplification (c) as functions of asymmetry ϕ_{eq} and viscosity ν in case of $Q_c = 0$ and idealized vertical diffusion. The contour intervals are 5×10^9 kg/s, 10×10^9 kg/s and 2, respectively.

and Phillips, 1990) while such a coupling is neglected in diagnostic models.

The 2D → 3D alteration of the zonal wind is characterized by reduction, broadening and poleward shift of the jet. This effect is related to eddy induced vorticity mixing into the poleward flow of the Hadley cell. We have given an empirical estimation ($\bar{\xi} \approx -f/2$, eq. (28)) which approximately applies to model and observational data.

The 2D → 3D alterations of the Hadley cell are generally associated with an intensification of the equatorward flow at low altitudes. In the upper troposphere the changes strongly depend on the amplitude of Q_c. (Q_c is maximum at 550 mb and confined to the intertropical convergence zone, see Fig. 1.) If no additional heating is applied ($Q_c = 0$), the 3D Hadley cell maximum is located at low altitudes (Fig. 2b). When switching from 2D to 3D, the entire Hadley circulation strikingly increases (Fig. 2), but nevertheless its strength amounts to less than one half of the observational value. If a realistic tropical heating rate is simulated with help of Q_c, the 2D → 3D alteration of the Hadley cell is twofold. In addition to low level intensification the upper level maximum of the meridional streamfunction (located at ~350 mb) is reduced by a factor of about 2 (Fig. 3).

In 2D, the basic assumptions of the analytical model of Held and Hou (1980) apply, i.e., angular momentum and energy are conserved within the zonally symmetric flow (Figs. 5, 8). Comparisons of 2D angular momentum and heat budgets with corresponding 3D results (Figs. 6, 9) indicate how Hadley cell and transient waves are locked. First, the eddies contribute to the angular momentum budget, giving rise to vorticity mixing and changes of the zonal wind jet as described above. Using the analytical model of Held and Hou, we have shown that vorticity mixing amplifies the entire Hadley circulation, which qualitatively applies in case of $Q_c = 0$. Second, cooling in subtropics due to eddy heat flux is in the main balanced by entropy advection of descending flow and exceeds diabatic cooling (Fig. 9). Switching from 2D to 3D always causes enhanced advection into low altitudes in order to balance the negative eddy heat flux convergence, resulting in vertical elongation of the Hadley cell. This mechanism is in accordance with the vorticity mixing argument in case of $Q_c = 0$. It also yields a qualitative explanation in case of strong Q_c: If we assume that deep tropical heating remains approximately the same from 2D to 3D, then enhanced advection into low altitudes can only be achieved by reduction of the high altitude circulation.

A detailed analysis to what extent the computational 3D heat budget applies to reality has not been done yet. We expect deviations due to stationary waves which have been excluded but are known to cause strong eddy fluxes in midlatitudes. Also vertical mixing of angular momentum due to cumulus convection (Schneider 1977) is not considered in our investigation. This process is known to alter the effective turbulent viscosity and hence may be crucial especially in 2D computations. Furthermore, neglection of moisture pro-

cesses and simulation of solar radiation by temperature relaxation are generally to be questioned. Nevertheless, the present results support the hypothesis that feedback of midlatitude waves onto the Hadley cell plays an important role in tropical–extratropical interactions.

7. Acknowledgement

We are indebted to Deutscher Wetterdienst and Deutsches Klimarechenzentrum for making available ECMWF-data. This work was partially supported by the Bundesministerium für Bildung, Wissenschaft, Forschung und Technologie 01LL9214. The comments of the reviewers are gratefully acknowleged.

8. Appendix

Parametrization of equilibrium temperature

In the following, a zonally symmetric temperature field

$$T_e = T_e(\varnothing, p; \ldots) \tag{A.1}$$

is introduced. $\varnothing$ denotes the latitude and p the pressure. The dependence on the free parameters which control the temperature distribution is indicated by ellipses. These free parameters are defined as:

- $\varnothing_{eq}$ latitude of the seasonal equator
- p_{bo} surface pressure
- p_{tr} pressure at the tropopause above the equator for $\varnothing_{eq} = 0$
- p_{to} top pressure level
- T_{eq} surface temperature at $\varnothing = 0$ for $\varnothing_{eq} = 0$
- T_{po} surface temperature at the poles for $\varnothing_{eq} = 0$
- T_{tr} temperature at the tropopause above the equator for $\varnothing_{eq} = 0$
- T_{to} temperature at the top pressure level above the equator for $\varnothing_{eq} = 0$
- $\varnothing_{je}$ latitude of the wind jets for $\varnothing_{eq} = 0$
- $s_\varnothing$ sharpness of the windjets with respect to latitude
- p_{je} pressure level of the wind jets for $\varnothing_{eq} = 0$
- s_p sharpness of the windjets with respect to pressure

We write T_e as a product of two functions

$$T_e(\varnothing, p; \ldots) = \zeta(p; \ldots) B(\varnothing, p; \ldots), \tag{A.2}$$

where ζ describes the main dependence of T_e on pressure and B the main dependence on latitude.

An appropriate meridional temperature gradient is achieved by

$$B(\varnothing, p; \ldots) = b_1 + b_2 \arctan\left(\frac{p - p_{je}}{s_p}\right) \times \left\{\frac{1}{2} - \arctan\left(\frac{S^2 - \sin^2 \varnothing_{je}}{s_\varnothing^2}\right) \Big/ \pi\right\}. \tag{A.3}$$

S equals $\sin \varnothing$ if the temperature is symmetric with respect to the equator ($\varnothing_{eq} = 0$). In general S is given by

$$S = \sin \varnothing - \left(\frac{p - p_{to}}{p_{bo} - p_{to}}\right) \sin \varnothing_{eq}. \tag{A.4}$$

The term $\{\ldots\}$ in (A.3) describes the latitude dependence of T_e at low altitudes. The term $\arctan((p - p_{je})/s_p)$ is such that the meridional temperature gradient changes sign at the jet level

With the assumption

$$\zeta(p = p_{bo}; \ldots) = 1, \tag{A.5}$$

b_1 and b_2 are defined by the surface temperatures at the equator and the poles for $S = \sin \varnothing$:

$$T_{eq} = b_1 + b_2 \arctan\left(\frac{p_{bo} - p_{je}}{s_p}\right) \times \left(\frac{1}{2} - \arctan\left(\frac{-\sin^2 \varnothing_{je}}{s_{je}^2}\right) \Big/ \pi\right), \tag{A.6}$$

$$T_{po} = b_1 + b_2 \arctan\left(\frac{p_{bo} - p_{je}}{s_p}\right) \times \left(\frac{1}{2} - \arctan\left(\frac{1 - \sin^2 \varnothing_{je}}{s_{je}^2}\right) \Big/ \pi\right). \tag{A.7}$$

In addition to (A.5) ζ has to fullfill

$$\zeta(p_{to}; \ldots) = T_{to}/B(0, p_{to}; \ldots) =: \zeta_{to}, \tag{A.8}$$

$$\zeta(p_{tr}; \ldots) = T_{tr}/B(0, p_{tr}; \ldots) =: \zeta_{tr}, \tag{A.9}$$

$$\partial_p \{B(0, p_{tr}; \ldots)\zeta(p_{tr}; \ldots)\} = 0, \tag{A.10}$$

with the constraint that B is evaluated for $\varnothing_{eq} = 0$.

The vertical temperature profile is parametrized by

$$\zeta(p; \ldots) = \zeta_0 + \frac{\zeta_1}{\bar{\omega} + p} + \frac{\zeta_2}{(\bar{\omega} + p)^2}. \tag{A.11}$$

The four coefficients ζ_0, ζ_1, ζ_2 and $\bar{\omega}$ depend on the temperature parameters and are eliminated in the following way. First, ζ_0, ζ_1 and ζ_2 are repres-

ented as functions of $\bar{\omega}$ using (A.5), (A.8) and (A.9):

$$\zeta_2 = \left\{ \frac{1-\zeta_{tr}}{(\bar{\omega}+p_{tr})^{-1}-(\bar{\omega}+p_{bo})^{-1}} - \frac{1-\zeta_{to}}{(\bar{\omega}+p_{to})^{-1}-(\bar{\omega}+p_{bo})^{-1}} \right\} \Big/ \{(\bar{\omega}+p_{to})^{-1}-(\bar{\omega}+p_{tr})^{-1}\},$$

$$\zeta_1 = -\frac{1-\zeta_{to}}{(\bar{\omega}+p_{to})^{-1}-(\bar{\omega}+p_{bo})^{-1}} - \zeta_2\{(\bar{\omega}+p_{to})^{-1}+(\bar{\omega}+p_{bo})^{-1}\},$$

$$\zeta_0 = 1 - \frac{1}{\bar{\omega}+p_{bo}}\left(\zeta_1 + \frac{\zeta_2}{\bar{\omega}+p_{bo}}\right). \quad \text{(A.12)}$$

Then, inserting (A.12) into (A.10), $\bar{\omega}$ is determined by the zero of the left-hand side of (A.10) and must be found numerically.

REFERENCES

Asselin, R. 1972. Frequency filter for time integrations. *Mon. Wea. Rev.* **100**, 487–490.

Barnes, J. R. and Young, R. E. 1992. Nonlinear baroclinic instability on the sphere: multiple life cycles with surface drag and thermal damping. *J. Atmos. Sci.* **49**, 861–878.

Chang, E. K. M. 1995. The influence of Hadley circulation intensity changes on extratropical climate in an idealized model. *J. Atmos. Sci.* **52**, 2006–2024.

Dethloff, K. and Schmitz, G. 1981. Zur Bestimmung der Meridionalzirkulation der Tropo- und Stratosphäre auf der Grundlage eines zonalsymmetrischen Modells. *Z. Meteorol.* **31**, 306–321.

Edmon, Jr., H. J., Hoskins, B. J.and McIntyre, M. E. 1980. Eliassen–Palm cross sections for the troposphere. *J. Atmos. Sci.* **37**, 2600–2615.

Held, I. M. and Hou, A. Y. 1980. Nonlinear axially symmetric circulations in a nearly inviscid atmosphere. *J. Atmos. Sci.* **37**, 515–533.

Held, I. M. and Phillips, P. J. 1990. A barotropic model of the interaction between the Hadley cell and a Rossby wave. *J. Atmos. Sci.* **47**, 856–869.

Holtslag, A. A. M. and Boville, B. A. 1993. Local versus nonlocal boundary-layer diffusion in a global climate model. *J. Climate* **6**, 1825–1842.

Hoskins, B. J.and Simmons, A. J. 1975. A multilayer spectral model and the semi-implicit method. *Quart. J. R. Met. Soc.* **101**, 637–655.

Hou, A. Y. 1993. The influence of tropical heating displacements on the extratropical climate. *J. Atmos. Sci.* **50**, 3553–3570.

Hou, A. Y. and Lindzen, R. S. 1992. The influence of concentrated heating on the Hadley circulation. *J. Atmos. Sci.* **49**, 1233–1241.

James, I. N. 1994. The Held–Hou model of the Hadley circulation. In: *Introduction to circulating atmospheres.* Cambridge University Press, pp. 85–92.

Laursen, L. and Eliasen, E. 1989. On the effects of the damping mechanisms in an atmospheric general circulation model. *Tellus* **41A**, 385–400.

Lindzen, R. S. 1994. The effect of concentrated PV gradients on stationary waves. *J. Atmos. Sci.* **51**, 3455–3466.

Lindzen, R. S. and Hou, A. Y. 1988. Hadley circulations for zonally-averaged heating centered off the equator. *J. Atmos. Sci.* **45**, 2416–2427.

Lorenz, E. N. 1967. The nature and theory of the general circulation of the atmosphere. *WMO Publ.* **218**.

Machenhauer B. and Rasmussen, E. 1972. On the integration of the spectral hydrodynamical equations by a transform method. *Report* no. **3**, Institute of theoretical meteorology, University of Copenhagen.

Pfeffer, R. L. 1981. Wave-mean flow interactions in the atmosphere. *J. Atmos. Sci.* **38**, 1340–1359.

Saravanan, R. 1993. Equatorial superrotation and maintenance of the general circulation in two-level-models. *J. Atmos. Sci.* **50**, 1211–1227.

Satow, M. 1994. Hadley circulations in radiative–convective equilibrium in an axially symmetric atmosphere. *J. Atmos. Sci.* **51**, 1947–1967.

Satow, M., Shiobara, M. and Takahashi, M. 1995. Hadley circulations and their roles in the global angular momentum budget in two- and three-dimensional models. *Tellus* **47A**, 548–560.

Schneider, E. K. 1977. Axially symmetric steady-state models of the basic state for instability and climate studies. Part II. Nonlinear calculations. *J. Atmos. Sci.* **34**, 280–296.

Simmons, A. J.and Burridge, D. M. 1988. An energy and angular-momentum conserving vertical finite-difference scheme and hybrid vertical coordinates. *Mon. Wea. Rev.* **109**, 758–766.

Ulbrich, U., Graf, H.-F. and Kirchner, I. 1995. The impact of El Niño and volcanic forcing on the atmospheric energy cycle and the zonal mean atmospheric ciculation. *Beitr. Phys. Atmosph.* **68**, 59–74.

Williams, G. P. 1988a. The dynamical range of global circulations (I). *Climate Dyn.* **2**, 205–260.

Williams, G. P. 1988b. The dynamical range of global circulations (II). *Climate Dyn.* **3**, 45–84.